

Rolling with the Punches: Resilient Contrastive Pre-training under Non-Stationary Drift

Xiaoyu Yang, Jie Lu*, En Yu

Australian Artificial Intelligence Institute (AAIL),
Faculty of Engineering and Information Technology,
University of Technology Sydney, Australia.
xiaoyuyang386@gmail.com

Abstract

The remarkable success of large-scale contrastive pre-training, fueled by vast and curated datasets, is encountering new frontiers as the scaling paradigm evolves. A critical emerging challenge is the effective pre-training of models on dynamic data streams characterized by concept drift—unpredictable changes in the underlying data distribution. This paper undertakes a foundational investigation of this issue. We first reveal that conventional contrastive pre-training methods are notably vulnerable to concept drift, leading to significant biases in the learned feature space of pre-trained models. To systematically analyze these effects, we construct a structural causal model that elucidates how drift acts as a confounder, distorting learned representations. Based on these causal insights, we propose Resilient Contrastive Pre-training (RCP), a novel method incorporating causal intervention. RCP introduces a causally-informed objective designed to mitigate drift-induced biases by leveraging targeted interventions. RCP is designed for simple and scalable implementation and exhibits notable adaptability, promoting robust and autonomous pre-training on evolving data. Comprehensive experiments across diverse downstream tasks compellingly demonstrate that RCP effectively alleviates the detrimental impact of concept drift, yielding more resilient and generalizable representations.

1 Introduction

Contrastive learning has proven to be a highly effective paradigm for pre-training large-scale models, particularly demonstrated by its success in large vision models, such as SimCLR [1, 2], MoCo [3, 4], DINO [5, 6]. However, the continued scaling of these models intensifies their data requirements, drawing significant attention to the challenge of pre-training effectively on data streams that exhibit concept drifts [7, 8], where the underlying data distribution evolves unpredictably during pre-training. In practical pre-training scenarios, this can manifest in various forms, encompassing issues such as evolving long-tailed distributions, noisy labels, or domain shifts. Hence, a pertinent question emerges: beyond the existing contrastive learning methods, *can contrastive paradigms learn from drift pre-training?* In this work, we aim to address this question through a systematic investigation. Our analysis reveals significant vulnerabilities in current contrastive pre-training methods when faced with evolving data distributions, underscoring the urgent need for novel strategies to enhance their robustness and adaptability in dynamic, real-world data environments. More related works are provided in Appendix A.

Current contrastive pre-training methods predominantly operate by maximizing agreement between two distinct views of the same input instance, often generated via data augmentation and processed

*Corresponding Author

through different encoders or network states [1, 9, 3]. In the context of large vision models, student-teacher architectures are prevalent, as seen in frameworks like DINO [5] and MoCo v3 [4]. Typically, the student network is propelled by the contrastive loss, whereas the teacher network is momentum updated through an exponential moving average (EMA) of the student parameters. However, this widely adopted momentum-based mechanism is particularly susceptible to the adverse effects of concept drift. As the input data distribution evolves, the slowly updating teacher network can accumulate biases from outdated distributions. This stale information, perpetuated by the momentum update, can lead to a progressively amplified misalignment between the learned representations and the current data characteristics.

To concretely illustrate this phenomenon, we examine the impact of long-tailed drift—a common manifestation of concept drift where class frequencies change over time—on the contrastive pre-training process. We visualize the feature space learned by MoCo v3 [4] in Fig.1. For this analysis, we simulate pre-training on two scenarios: one using the standard, balanced ImageNet dataset [10] and another using ImageNet-LT [11] to represent a long-tailed data stream. The feature visualizations are generated using a balanced test set to ensure fair comparison. Categories are differentiated by varying colors ranging from dark to light, indicating a spectrum from categories with few training samples to those with abundant samples. As depicted in Fig.1b (the long-tailed drift scenario), the feature space becomes highly skewed. Tail categories are compressed into a diminutive region, while head categories, benefiting from their over-representation in the training stream, dominate the majority of the space. This distortion steers the learned feature manifold away from the more uniform structure observed when training on balanced data (Fig.1a). Such undesirable behavior can be attributed to the accumulated bias in the momentum-updated teacher network, which has been predominantly exposed to head classes, provides suboptimal guidance for learning representations of tail classes as the distribution drifts.

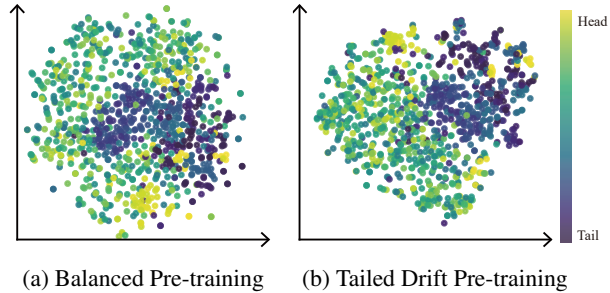


Figure 1: The t-SNE visualization of feature space under the different conditions of pre-training within ImageNet and ImageNet-LT. The dark colors signify the region corresponding to the tail category with limited pre-training samples, whereas light colors denote the head category characterized by abundant samples.

Building the above analysis, we formalize the interplay between these components using a Structural Causal Model (SCM), depicted in Fig.2a. It elucidates the causal relationships among input samples X , predictions Y , the latent concept drift D inherent in the data stream, and the bias B that accumulates in the momentum-updated teacher network [12]. Our causal analysis (detailed in Section 2.1) reveals that concept drift D acts as a critical confounder. It not only influences the input features X ($D \rightarrow X$) but also shapes the bias B within the teacher network ($X, D \rightarrow B$), which in turn affects Y , i.e., $(X, B) \rightarrow Y$. This creates a spurious backdoor path $X \leftarrow D \rightarrow B \rightarrow Y$ that can mislead the learning process by inducing false correlations between X and Y . Furthermore, the mediation [13] path $X \rightarrow B \rightarrow Y$ confounds the direct contribution of $X \rightarrow Y$, as detailed in Section 2.1.

These causal insights underscore the limitations of standard contrastive methods in drifting environments. Therefore, to address the detrimental effects of such confounding and biased mediation, we propose a novel pre-training method, **Resilient Contrastive Pre-training (RCP)**. Our approach leverages causal intervention techniques [14] to mitigate the bias B propagated by concept drift D , thereby enabling more robust and generalizable representation learning from non-stationary data streams. In summary, our paper mainly makes the following contributions:

1. We are pioneers in uncovering how concept drift impacts contrastive pre-training, specifically identifying the accumulation of bias through the momentum update mechanism. This foundational understanding paves the way for future research into robust pre-training on large-scale, dynamic datasets.
2. Leveraging insights from our structural causal model, we propose causal interventional contrastive pre-training (RCP), a novel method that employs causal intervention to mitigate

drift-induced bias. RCP is designed to be straightforward to implement and scalable, making it suitable for pre-training large models on evolving data streams.

3. Extensive experiments demonstrate the superiority of RCP across diverse downstream tasks, e.g., long-tailed classification, OOD detection, and domain adaptation, using both fine-tuning and linear probing evaluation protocols. Notably, our analysis of inter-category distances in the learned feature space confirms that RCP effectively mitigates the detrimental effects of drift, leading to more discriminative and robust representations for large-scale pre-training.

2 Methodology

2.1 Causal Lens on Contrastive Drift Pre-training

Contrastive Drift Pre-training (CDP). Concept drift is a statistical phenomenon wherein the joint distribution $P(X, Z)$ of features X and target variables Z evolves over time [7]. We define Drift Pre-training as a pre-training paradigm operating on a data stream $\mathcal{S}_{0,T} = \{S_0, S_1, \dots, S_T\}$. Each element $S_t = \{(x_i, z_i)\}_{i=1}^{n_t}$ consists of n_t samples with feature vector x_i and an associated contrastive label z_i at timestamp t . This timestamp t also corresponds to an iteration in the pre-training process. At any given iteration t , data samples $\{X, Z\} \in \{(x_i, z_i)\}_{i=1}^{n_t}$ are drawn from a joint distribution $P_t(X_t, Z_t)$. Concept drift within this pre-training context is then formally characterized by:

$$\exists t \in [0, T): P_t(X, Z) \neq P_{t+1}(X, Z), \quad (1)$$

where the joint probability $P_t(X, Z)$ can be decomposed as $P_t(X, Z) = P_t(X) \times P_t(Z|X)$. Therefore, concept drift theory provides a unified framework to harmonize the tailed shift and OOD shift that often occur together, enabling more robust and adaptive deep learning models.

CDP investigates contrastive learning under such non-stationary conditions, typically employing momentum-updated teacher-student frameworks [3], i.e.,

$$\theta_t^m = \lambda \theta_{t-1}^m + (1 - \lambda) \theta_{t-1}^g, \quad (2)$$

where θ^m signifies the parameters of the teacher network, θ^g denotes those of the student network, and $\lambda \in [0, 1)$ represents the momentum coefficient. Momentum $\lambda \theta_{t-1}^m$ induces a slower evolution of the teacher network θ^m relative to the student network θ^s . While high momentum (e.g., $\lambda = 0.999$ [4]) stabilizes training on stationary data, it poses a significant challenge under concept drift: the slowly updating teacher network θ^m can become severely misaligned with the current data distribution $P_t(x, z)$, thereby accumulating stale biases from past distributions and hindering the model's ability to adapt to new or evolved concepts present in the current iteration S_t .

Objective. Therefore, CDP aims to enable the learning system to synchronize with the evolving data distribution, ensuring that the pre-training model accurately reflect the current state of the data. We formalize this objective as maximizing the agreement between the student model and momentum model over a prospective adaptation window $[t, t + \tau]$:

$$\max_{\{g_j^\theta\}_{j=t}^{t+\tau}} \sum_{j=t}^{t+\tau} \mathcal{L}_{\text{agree}}(g_j^\theta(\tilde{X}_j), m_j^\theta(\hat{X}_j)) \quad (3)$$

where \tilde{X}_j and \hat{X}_j symbolize different augmented samples obtained from X_j , g_j^θ denotes the student model trained by the data stream $S_{j-\tau, j-1}$ from the drift adaptation window with the size of τ , and m_j^θ represents the momentum model. And the pre-training is driven by the target metric $\mathcal{L}_{\text{agree}}$ to continuously adapt the drift in a given drift adaptation window of $[t, t + \tau]$ time period.

Causal Analysis of CDP. To further understand the challenges posed by concept drift in CDP, we employ a Structural Causal Model (SCM) [15, 14]. As shown in Figure 2, the constructed causal graph of $\{X, Y, D, B\}$ presents the following causal connections:

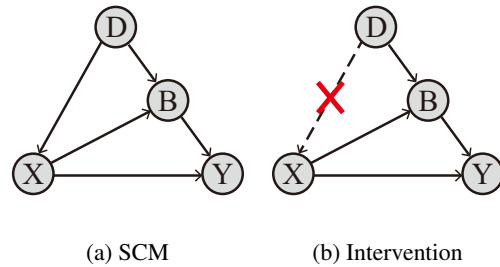


Figure 2: The proposed causal graph of contrastive pre-training. **X**: Sample Features, **Y**: Prediction, **D**: Latent Concept Drift within Data Streams, and **B**: Sample Bias in the Momentum Update.

$D \rightarrow X$: X denotes features extracted by samples drawn from the data stream with concept drift D , which is obviously trained under the effect of the drift pre-training.

$(X, D) \rightarrow B$: B represents the sample bias deviated from feature X under the effect of the concept drift D within the data stream. In the context of drift pre-training, the bias will accumulate during the momentum update of the teacher network, which will be amplified in the subsequent iteration of the contrastive pre-training.

$(X, B) \rightarrow Y$: This link presents that, apart from the regular $X \rightarrow Y$, the prediction is also impacted by the concept drift within the data stream through the mediation bias of B .

In the constructed causal graph, nodes D and B are identified as the confounder and the mediator [13], respectively. The confounder D influences both the independent variable X and the outcome variable Y from the backdoor path $X \leftarrow D \rightarrow B \rightarrow Y$, thereby distorting the estimated effect of the sample features on the predictions and resulting in the spurious correlation. For example, in the case of long-tailed drift pre-training, tail samples may be incorrectly associated with head categories through this backdoor path, a misalignment attributable to this spurious correlation. Besides, mediator B conveys the drift effect of sample features X on predictions Y via the pathway $X \rightarrow B \rightarrow Y$, weakening the direct impact of X on Y .

2.2 Causal Interventional Contrastive Objective

Drawing from the aforementioned causal relationships, it can be argued that current contrastive pertaining approaches involving the InfoNCE loss [16] essentially leverages the likelihood $P(Y|X)$ to drive the whole network, which is vulnerable by the concept drift confounder D and leads to the emergence of spurious correlations. By marginalizing over the discrete drift contexts $D = \{d_1, \dots, d_{|D|}\}$ [17], $P_t(Y|X)$ can be expressed as:

$$P_t(Y|X) = \sum_{i=1}^{|D|} P_t(Y|X, B = h(X, d_i))P_t(d_i|X) \quad (4)$$

where $B = h(X, d)$ represents the sample bias B conditioned on features X and a specific drift context d_i . Following the [18], d_i is simplified to the drift of the latent category center underlying the pre-training. The term $P_t(d|X)$ highlights how X might carry information about d .

Inspired by recent advancements in applying causal inference to deep learning [19, 20, 21], we employ causal intervention $P_t(Y|\text{do}(X))$ to cut off the pathway of $D \rightarrow X$ at timestamp t in drift data stream as illustrated in Fig. 2b, where $\text{do}(\cdot)$ denotes the interventional operation [14, 22]. In accordance with the backdoor adjustment, the de-confounding operation $\text{do}(X)$ involves stratifying the confounder into discrete segments $D = \{d_1, d_2, \dots, d_{|D|}\}$, thereby rendering D no longer a confounder between X and Y . Thus, $P_t(Y|\text{do}(X))$ can be expressed as:

$$P_t(Y|\text{do}(X)) = \sum_{i=1}^{|D|} P_t(Y|X, B = h(X, d_i))P_t(d_i) \quad (5)$$

In Eq. (5), $P_t(Y|\text{do}(X))$ compels X to equally consider each confounding factor d_i and integrate them collectively to predict Y . Through this approach, the original classifier $P_t(Y|X)$ is replaced by $P_t(Y|\text{do}(X))$ at the iteration t , as shown:

$$P_t(Y|\text{do}(X)) \triangleq P_t(Y|X) \quad (6)$$

The de-confound classifier mitigates the confounding influence and captures the genuine causality from X to Y , thereby enhancing the quality of the contrastive pre-training. Nevertheless, Eq. (5) necessitates costly sampling to approximate $P(Y|\text{do}(X))$ when implementing it in contrastive pre-training, resulting in impractical training times. Fortunately, the Normalized Weighted Geometric Mean (NWGM) [23, 24, 25] explores an alternative to approximate Eq. (5) in a single feed-forward process as following:

$$P_t(Y|\text{do}(X)) \approx P_t(Y|X, B = \sum_{i=1}^{|D|} h(X, d_i)P_t(d_i)) \quad (7)$$

As a result, according to the interventional probability outlined in Eq. (7), contrastive pre-training is compelled to grasp the genuine causal effect: $X \rightarrow Y$ rather than the misleading correlations induced by the concept drift confounder D . Thus, combined with Eq. (3), the final interventional contrastive pre-training objective is formulated as:

$$\begin{aligned}\mathcal{L}_{\text{agree}}(g_j^\theta(\tilde{X}_j), m_j^\theta(\hat{X}_j)) &= P_t(Y|X, \sum_{i=1}^{|D|} h(X, d_i) P_t(d_i)) \\ &= P_t(Y|g(\tilde{X}_j), \text{Softmax}(h(g_j^\theta(\tilde{X}_j) m_j^\theta(\hat{X}_j))))\end{aligned}\quad (8)$$

2.3 Resilient Contrastive Pre-training

To realize the causal interventional objective for CDP, we introduce **Resilient Contrastive Pre-training (RCP)**, an approach tailored for learning from data streams exhibiting concept drift. As depicted in Fig. 3, RCP adapts the student-teacher architecture of MoCo v3 [4], utilizing an encoder (g) and a momentum encoder (m). Within each drift adaptation window $[t, t + \tau]$, two augmented views (\tilde{x}, \hat{x}) are generated per image. The student encoder g processes one view into features $v = g(\tilde{x})$, which an MLP head then projects into a query $q = h(v)$. The momentum encoder m , structurally identical to g and updated via EMA (Eq. (2)), processes the other view to produce a key $k = m(\hat{x})$, ensuring stable targets and enhancing training stability. Central to RCP is an intervention module that processes q , v , and k to mitigate latent biases from concept drift. This module computes an interventional score component $c = \text{Softmax}(q \cdot k) \cdot v$, which embodies aspects of our causal objective (Eq. (8)). The overall network is then trained using an InfoNCE loss [16]:

$$\mathcal{L} = -\log \frac{\exp(c_1 \cdot c_2^{i+}/\tau)}{\sum_{i=t}^{t+\tau} \exp(c_1 \cdot c_2^i/\tau)}, \quad (9)$$

where τ is a temperature hyper-parameter [26]. The sum is over one positive and all negative samples within the drift adaptation window $[t, t + \tau]$ of the data stream.

Intuitively, q akin to a "query" [3], the momentum output k acts as the "key" for sampling key drift of the data stream, and the "value" v resembles a blend of the essential contrastive object and the concept drift. Therefore, the goal of causal intervention is to mitigate the bias of the contrastive objective through the drift sampling within the adaption window. We find the derived causal intervention module has a similar structure to the self-attention mechanism [27]. Thus, this query-key-value mechanism structurally resembles self-attention [27], suggesting an inherent capability to model contextual dependencies useful for tracking drift. However, it is important to highlight that we employ "key" and "query" sampling for concept drift within the data stream to mitigate bias in the "value", which is different from the aim of sequence position modelling in the self-attention mechanism.

Besides, our RCP method is simple to implement, efficient and scalable, with more details provided in Appendix.B.

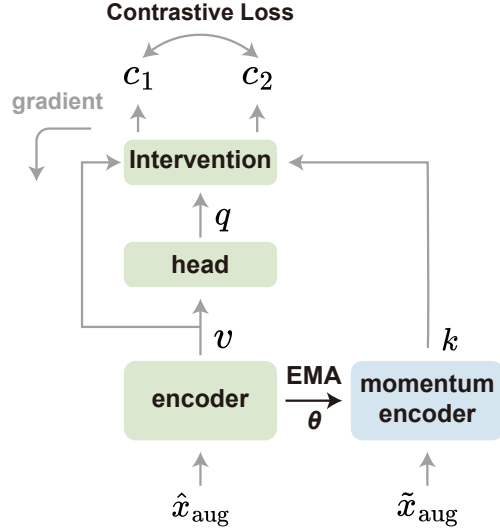


Figure 3: **The workflow of our causal contrastive pre-training under concept drift streaming.** Within the data streaming, a large batch size is opted for a wider drift adaptation window sliding to adapt changes in data distribution. Undergoes various random augmentations, the transformed instances from the identical sample are feature-extracted by both the encoder and the momentum encoder to get the key and value, respectively. An MLP head is utilized to obtain the query of the encoder features. Subsequently, causal intervention is utilized to alleviate concept drift in the data stream within the adaptation window, resulting in the acquisition of two objects for contrastive learning.

Table 1: Evaluation results of fine-tuning on long-tailed classification tasks with ImageNet-LT [11] and iNaturalist2018 [28]. The best-performing contrastive pre-training results are highlighted in red. Many, Medium and Few denote the evaluated splits of many-shot (>100 training samples), medium-shot (20-100 samples) and few-shot (<20 samples). Top-1 accuracy is applied to evaluate the performance of different methods. † denotes methods that are adjusted for the long-tailed fine-tuning.

Methods	Backbones	ImageNet-LT				iNaturalist2018			
		Many	Medium	Few	All	Many	Medium	Few	All
Training from scratch									
cRT [29]	ResNet-50	61.8	46.2	27.3	49.6	69.0	66.0	63.2	65.2
LWS [29]		60.2	47.2	30.3	49.9	65.0	66.3	65.5	65.9
RIDE [30]		68.2	53.8	36.0	56.9	70.9	72.4	73.1	72.6
PaCo [31]		68.2	58.7	41.0	60.0	70.3	73.2	73.6	73.2
Masked Image Modeling Pre-training									
MAE [32]	ViT-B/16	74.7	48.2	19.4	54.5	79.6	70.8	65.0	69.4
LiVT † [33]		73.6	56.4	41.0	60.9	78.9	76.5	74.8	76.1
Contrastive Learning Pre-training									
ViT [34]	ViT-B/16	50.5	23.5	6.9	31.6	65.4	55.3	50.9	54.6
DeiT [35]		70.4	40.9	12.8	48.4	72.9	62.8	55.8	61.0
BYOL [9]		30.6	8.6	0.9	15.9	28.4	22.6	24.5	24.0
DINO [5]		64.8	35.5	11.3	43.3	76.7	67.1	61.2	65.5
DINO v2 [6]		68.4	36.9	11.7	45.4	71.9	62.7	58.2	61.6
MoCo v3 [4]		70.8	40.7	14.3	48.5	76.6	65.8	62.8	65.6
Ours		72.2	43.1	16.0	50.3	77.7	68.7	63.8	67.5

3 Experiments

In this section, we initially showcase the robust performance of our RCP in the downstream task of long-tailed classification under drift pre-training, with results of fine-tuning and linear probing. Subsequently, from the perspective of generalization, we conduct experiments of out-of-distribution (OOD) detection and domain shift, to assess the resilience of the model against gradual drift and sudden drift. Following that, the feature embedding space of pre-trained models is intuitively visualized with degrees, illustrating how RCP mitigates the concept drift within the feature space. Finally, we present the scaling ability of our method facing with the drift pre-training. More detailed experimental implementations are given in Appendix C.2.

3.1 Navigating Tailed Drift Pre-training

We compare our proposed RCP method with other models to explicitly demonstrate its superior performance in tailed drift pre-training. Two large-scale datasets, namely the ImageNet-LT [11] and iNaturalist 2018 [28] are utilized as source datasets to perform pre-training, fine-tuning and linear probing, respectively. To effectively illustrate the efficacy of RCP in mitigating tail drift, we follow the criterion and metrics of long-tailed classification [36] to report the Top-1 accuracy across various splits, including Many split with over 100 training samples, Medium split with 20-100 training samples, and Few split with fewer than 20 training samples.

Table 2: Evaluation results of linear probing on long-tailed classification tasks with ImageNet-LT and iNaturalist2018. The best-performing models are highlighted in red.

Methods	Many	Medium	Few	All
ImageNet-LT [11]				
BYOL [9]	8.5	0.5	0.1	3.5
DINO [5]	47.4	20.5	0.1	27.9
DINO v2 [6]	49.4	23.4	5.7	30.8
MoCo v3 [4]	45.8	18.7	0.0	27.1
Ours	52.7	24.0	7.9	32.8
iNaturalist2018 [28]				
BYOL [9]	7.0	3.1	2.5	3.2
DINO [5]	43.1	33.5	32.3	34.0
DINO v2 [6]	36.3	30.2	30.0	30.7
MoCo v3 [4]	32.9	25.4	22.4	24.9
Ours	48.4	37.0	35.1	37.3

In terms of fine-tuning results shown in Table 1, we compare mainstream contrastive pre-training methods, namely DeiT [35], BYOL [9], DINO [5], DINO v2 [6], MoCo v3 [4] with the baseline of ViT [34], and our RCP exhibits superior results beyond other contrastive pre-training methods. Compared to other methods that employ the student-teacher paradigm, such as BYOL, DINO, DINO v2, and MoCo v3, our RCP method demonstrates additional performance enhancements on both the Medium and Few splits, especially in the iNaturalist2018 dataset. It is demonstrated that the proposed causal interventional objective significantly alleviates the accumulated bias due to momentum updates of the teacher network. Meanwhile, under the concept drift scenario, BYOL without negative sample pairs has the inferior performance of long-tailed classification to the baseline ViT, while it is not noticeable in equilibrium [4]. We argue that, in drift pre-training, the essence of negative sample pairs is similar to the causal interventional objective, taking into account the causal relationship of all drifts for each positive sample like de-confounding operation in Eq. (5) to delineate the boundary of the feature space. Relying solely on maximizing positive agreement as a pre-training strategy will cause the model to be overwhelmed by the head category, eventually exacerbating concept drift.

Besides, we also provide other fine-tuning results of long-tailed classification under scratch training and masked image modelling pre-training for comprehensive analysis, as shown in Table 1. It is worth noting that our focus is on the impact of drift environments on contrastive pre-training. Therefore, we exclusively utilized RCP solely during the pre-training phase, without making any adjustments to the downstream classification tasks. Consequently, in comparison to other methods, all contrastive pre-training approaches exhibit relatively lower performance. In the context of the masked image modeling strategy, it is found that contrastive learning is more susceptible to concept drift in the data stream. We attribute it to the fact that contrastive learning relies more heavily on global information within the data flow to construct feature representations.

Furthermore, we provide linear probing results of contrastive pre-training methods in Table 2. It is evidenced that our resilient contrastive learning method outperforms other contrastive pre-training methods, corroborating our main contributions of causal interventional contrastive objective for drift pre-training. It is noteworthy that on the Few split of ImageNet-LT, several contrastive learning methods failed to perform effectively, whereas we attained an accuracy of 7.9%. It indicates that our approach can accurately construct feature representations for tail categories even in the presence of concept drift.

3.2 Taming OOD Drift and Domain Drift in Downstream Tasks

To validate the generalization capability of our RCP under concept drift scenarios, we conducted experiments from perspectives of domain shift and out-of-distribution (OOD) detection.

In terms of domain shift generalization as exhibited in Table 3, our primary focus is to assess the extent of the drift environment on the feature representation constructed during pre-training. Therefore, we select three subsets of ImageNet [10] to validate the domain shift performance, namely, ImageNet-V2 [37], ImageNet-Sketch [38] and ImageNet-R [39]. Our results achieve superior results across three datasets, investigating the effectiveness of the proposed RCP method. It corroborates that, the feature space we construct in pre-training abstracts and captures the essential information of images, while disregarding any unexpected interference from the

Table 3: Evaluation results of domain shift on ImageNet-V2 [37], ImageNet-Sketch [38] and ImageNet-R [39]. The best-performing models are highlighted in red. Top-1/-5 accuracy are applied to evaluate the performance of different methods.

Methods	Many	Medium	Few	Top-1	Top-5
ImageNet-V2 [37]					
BYOL [9]	29.7	7.8	1.0	15.2	31.8
DINO [5]	63.4	33.6	11.6	41.9	65.1
DINO v2 [6]	66.6	35.4	11.9	44.0	66.9
MoCo v3 [4]	62.9	37.3	12.6	43.1	66.0
Ours	69.7	41.2	14.9	48.3	72.1
ImageNet-Sketch [38]					
BYOL [9]	1.9	0.2	0.0	0.8	2.8
DINO [5]	12.4	5.0	0.5	7.1	16.2
DINO v2 [6]	17.1	6.8	1.4	9.9	20.8
MoCo v3 [4]	17.6	7.6	1.4	10.4	21.9
Ours	22.2	9.7	2.3	13.4	27.0
ImageNet-R [39]					
BYOL [9]	4.2	1.7	0.0	2.7	6.8
DINO [5]	13.4	7.6	0.4	9.5	18.3
DINO v2 [6]	15.8	8.6	0.7	11.1	21.1
MoCo v3 [4]	17.2	9.8	1.0	12.3	22.8
Ours	21.3	12.5	1.6	15.5	27.5

concept drift within the data stream. Moreover, judging from the results of Few split in ImageNet-Sketch and ImageNet-R, the majority of contrastive pre-training methods struggle to differentiate the tail categories. This difficulty arises from two main challenges. First, the bias induced by tail drift tends to skew models toward favoring head categories. On the flip side, the small sample size of tail categories limits the ability of pre-training methods to accurately extract their fundamental features, a problem that is exacerbated in the presence of domain shifts. Accordingly, our outstanding results demonstrate our proficiency in mitigating tail drift and extracting crucial features from limited samples.

Concerning out-of-distribution (OOD) detection, we also evaluate the capability of our RCP approach to delineate the boundaries of the feature space. While exhibiting slightly lower performance than DINO on ImageNet-O, we significantly outperform contrastive pre-training methods on the other three out-of-distribution datasets, and surpasses other approaches in overall performance. It demonstrates that our model possesses the benefits of intra-class compactness and inter-class separability in feature representation. Meanwhile, it is worth noting that in larger-scale balanced pre-training datasets, such as ImageNet-21k [40], our approach outperforms numerous traditional OOD detection methods in overall performance, such as ViM [41]. It underscores our RCP method can effectively alleviate concept drift bias in the model while also enhancing the characterization of the model’s decision boundary.

Table 4: Evaluation results of OOD detection with the OOD datasets of Texture [42], iNat-OOD [43, 44], ImageNet-O [45] and OpenImage-O [46]. ViT-B/16 is selected as the image encoder. The best-performing method is highlighted in red. FPR↓ and AUROC↑ are applied to evaluate the performance of different methods. PT denotes the pre-training dataset, where ‘-21k’ and ‘-1k’ represent ImageNet-21k [40] and ImageNet-1k [10], respectively. ID means the in-distribution dataset, where ‘-LT’ symbolizes ImageNet-LT [11].

Methods	PT	ID	Texture		iNaturalist		ImageNet-O		OpenImage-O		Overall	
			AUROC	FPR	AUROC	FPR	AUROC	FPR	AUROC	FPR	AUROC	FPR
MSP [47]			71.3	77.1	90.7	43.7	60.8	90.6	84.3	61.8	76.8	68.3
Energy [48]			54.1	86.3	76.6	72.7	61.6	81.0	71.1	74.0	65.9	78.5
MaxLog [49]			67.2	78.0	89.9	45.6	61.7	88.6	82.7	62.5	75.4	68.7
KL [49]			82.6	67.3	87.6	69.7	66.6	88.2	84.3	74.2	80.3	74.8
Residual [41]			82.4	64.6	73.7	86.0	68.4	87.5	74.9	78.0	74.9	79.0
React [50]		-21K -1K	62.1	80.5	91.2	38.7	63.7	81.0	80.4	60.4	74.3	65.2
Mahalanobis [51]			84.9	66.1	84.9	81.6	71.5	88.9	84.2	74.7	81.4	77.8
ViM [41]			83.5	62.7	77.8	81.7	71.0	86.6	78.3	74.6	77.7	76.4
MOODv1 [52]			93.0	30.9	98.8	5.9	86.8	63.2	95.5	26.5	93.5	31.6
MOODv2 [53]			94.3	24.7	99.6	1.8	91.5	40.8	97.4	13.6	95.7	20.2
BYOL [9]			58.4	92.1	80.1	77.5	52.0	92.2	65.3	81.3	64.0	85.8
DINO [5]		-LT -LT	72.9	80.7	85.7	65.3	74.2	80.2	74.7	83.0	76.9	77.3
DINO v2 [6]			67.1	85.1	78.9	88.4	63.1	88.3	73.9	85.4	70.7	86.8
MoCo v3 [4]			81.5	63.9	80.1	68.6	65.0	91.0	69.9	84.2	74.1	76.9
Ours			83.1	57.8	88.0	67.7	70.1	82.9	75.5	78.3	79.2	71.7

3.3 Boosting Pre-training Feature Embedding

To directly and intuitively demonstrate the feature space of the pre-trained model, we quantitatively calculate the feature embedding distances from three perspectives: In-Distribution (ID) intra-class compactness, ID inter-class separability, and the separability between ID and OOD categories, as shown in Table 5. Intra-class compactness within the In-Distribution (ID) measures the average distance between the category center and samples. ID Inter-class separability evaluates the distances between centers of different categories. Lastly, we assess the separability between ID categories and OOD samples.

The intra-class compactness results demonstrate that our model effectively validates the efficacy of the proposed RCP in delineating feature boundaries, especially in long-tailed scenarios. Moreover, the inter-class separability among different splits is very similar, suggesting that the pre-training

Table 5: Evaluation results of different contrastive learning strategies in the stage of pre-training, from three perspectives: ID intra-class compactness, ID inter-class separability and the separability between ID and OOD categories. The cosine metric is utilized to measure these distances, which is expressed as average degrees. ImageNet-LT is utilized for pre-training. The best-performing models are highlighted in red.

Pre-training	ID Intra Compactness ↓				ID Inter Separability ↑				ID vs. OOD Separability ↑			
	Many	Med.	Few	All	Many	Med.	Few	All	Many	Med.	Few	All
BYOL [9]	53.1	59.1	59.9	56.9	81.5	79.2	78.3	80.0	75.7	71.9	70.3	73.1
DINO [5]	34.2	51.4	59.0	45.9	89.0	88.4	87.6	88.5	86.2	84.4	81.4	84.7
DINO v2 [6]	31.2	50.1	57.8	43.9	88.9	88.1	87.2	88.3	86.0	83.7	80.5	84.1
MoCo v3 [4]	29.1	47.8	57.8	42.8	89.3	88.8	88.2	88.9	86.9	85.7	83.0	85.8
Ours	28.5	46.5	55.8	40.9	89.4	89.0	88.4	89.1	87.1	86.1	83.4	86.1

primarily influences intra-class compactness rather than inter-class separability. Furthermore, with the exception of BYOL, the inter-class separability of the other contrastive pre-training methods is nearly the same. This observation underscores the significance of negative samples in expanding inter-class separation. It also demonstrates that the bias is induced by accumulated drift within momentum updates, where features of head categories dominated the whole model under tailed drift. In the context of ID vs. OOD separability, we attained the optimal results, signifying that our feature space exhibits distinct feature boundaries. In addition, we find that the performance of ID vs. OOD separability aligns with the ID intra-class compactness, suggesting that enhancing the model’s performance hinges on mitigating data stream drift to enhance feature extraction capabilities.

3.4 Scaling with Drift Pre-training

To showcase the scalability of our RCP approach in scenarios involving concept drift, we evaluate the efficiency and scalability of our model in Table 6. As the number of parameters in ViT increases, our model exhibits a scalable effect, leading to performance improvements with larger models in downstream long-tailed classification tasks. In comparison to ViT-S/16, our proposed resilient contrastive learning method achieves nearly a 4% enhancement with ViT-B/16. This suggests that we can effectively train larger models to attain superior performance in the face of concept drift within data streams.

More critically, our experiments reveal that pre-trained models exhibit consistent scaling behavior even on datasets with great distribution drift. It demonstrates that our proposed RCP can effectively leverage larger-scale, minimally curated datasets, thereby substantially expanding the pool of usable data for pre-training without relying on complicated cleaning procedures.

Table 6: Evaluation results of scaling ability of our RCP on ImageNet-LT with ViT-Small/16, ViT-Base/16 and ViT-Large/16. Top-1 accuracy is utilized to evaluate the performance.

Backbones	ImageNet-LT			
	Many	Medium	Few	All
ViT-S/16	67.7	39.6	11.6	46.4
ViT-B/16	72.2	43.1	16.0	50.3
ViT-L/16	73.8	45.0	16.9	52.0

4 Conclusion and Outlooks

In this paper, we present resilient contrastive pre-training (RCP), a novel, straightforward and effective pre-training paradigm tailored for concept drift data stream. We employ causal inference theory to methodically examine the source of bias in the momentum update of contrastive pre-training and put forward a causal interventional objective to mitigate this bias within the drifting data stream. By virtue of this objective, RCP is devised to counteract the unpredictable distribution changes occurring within the data stream.

We hope that our work will inspire future advancements in contrastive pre-training paradigm, specifically addressing biases originating from real-world data challenges. In future research, we will leverage causal inference to analyze mixture of concept drift in pre-training.

References

- [1] Chen, T., S. Kornblith, M. Norouzi, et al. A Simple Framework for Contrastive Learning of Visual Representations. In *Proceedings of the 37th International Conference on Machine Learning*, pages 1597–1607. PMLR, 2020.
- [2] Chen, T., S. Kornblith, K. Swersky, et al. Big Self-Supervised Models are Strong Semi-Supervised Learners, 2020.
- [3] He, K., H. Fan, Y. Wu, et al. Momentum Contrast for Unsupervised Visual Representation Learning. In *Proceedings of the IEEE/CVF Conference on Computer Vision and Pattern Recognition*, pages 9729–9738. 2020.
- [4] Chen, X., S. Xie, K. He. An Empirical Study of Training Self-Supervised Vision Transformers. In *Proceedings of the IEEE/CVF International Conference on Computer Vision*, pages 9640–9649. 2021.
- [5] Caron, M., H. Touvron, I. Misra, et al. Emerging Properties in Self-Supervised Vision Transformers. In *Proceedings of the IEEE/CVF International Conference on Computer Vision*, pages 9650–9660. 2021.
- [6] Zhou, G., H. Pan, Y. LeCun, et al. DINO-WM: World Models on Pre-trained Visual Features enable Zero-shot Planning, 2024.
- [7] Lu, J., A. Liu, F. Dong, et al. Learning under Concept Drift: A Review. 31(12):2346–2363, 2019.
- [8] Yang, X., J. Lu, E. Yu. Adapting multi-modal large language model to concept drift from pre-training onwards. *arXiv preprint arXiv:2405.13459*, 2024.
- [9] Grill, J.-B., F. Strub, F. Altché, et al. Bootstrap Your Own Latent - A New Approach to Self-Supervised Learning. In *Advances in Neural Information Processing Systems*, vol. 33, pages 21271–21284. Curran Associates, Inc., 2020.
- [10] Russakovsky, O., J. Deng, H. Su, et al. Imagenet large scale visual recognition challenge. 115(3):211–252, 2015.
- [11] Liu, Z., Z. Miao, X. Zhan, et al. Large-Scale Long-Tailed Recognition in an Open World. In *Proceedings of the IEEE/CVF Conference on Computer Vision and Pattern Recognition*, pages 2532–2541. IEEE, 2019.
- [12] Pearl, J. Interpretation and identification of causal mediation. *Psychological methods*, 19(4):459, 2014.
- [13] —. Direct and indirect effects. In *Probabilistic and causal inference: the works of Judea Pearl*, pages 373–392. 2022.
- [14] —. *Causal inference in statistics: a primer*. John Wiley & Sons, 2016.
- [15] —. Causal diagrams for empirical research. *Biometrika*, 82(4):669–688, 1995.
- [16] Oord, A. v. d., Y. Li, O. Vinyals. Representation learning with contrastive predictive coding. *arXiv preprint arXiv:1807.03748*, 2018.
- [17] Tang, K., J. Huang, H. Zhang. Long-Tailed Classification by Keeping the Good and Removing the Bad Momentum Causal Effect. In *Advances in Neural Information Processing Systems*. 2021.
- [18] Deng, X., Z. Zhang. Comprehensive Knowledge Distillation with Causal Intervention. In *Advances in Neural Information Processing Systems*, vol. 34, pages 22158–22170. Curran Associates, Inc., 2021.
- [19] Lv, F., J. Liang, S. Li, et al. Causality Inspired Representation Learning for Domain Generalization. In *Proceedings of the IEEE/CVF Conference on Computer Vision and Pattern Recognition*, pages 8046–8056. 2022.
- [20] Choi, S., M. Jeong, H. Han, et al. C2L: Causally Contrastive Learning for Robust Text Classification. 36(10):10526–10534, 2022.
- [21] Rohekar, R. Y., Y. Gurwicz, S. Nisimov. Causal Interpretation of Self-Attention in Pre-Trained Transformers. 36:31450–31465, 2023.

- [22] Pearl, J., et al. Models, reasoning and inference. *Cambridge, UK: CambridgeUniversityPress*, 19(2):3, 2000.
- [23] Xu, K., J. Ba, R. Kiros, et al. Show, Attend and Tell: Neural Image Caption Generation with Visual Attention, 2016.
- [24] Liu, B., D. Wang, X. Yang, et al. Show, Deconfound and Tell: Image Captioning With Causal Inference. In *Proceedings of the IEEE/CVF Conference on Computer Vision and Pattern Recognition*, pages 18041–18050. 2022.
- [25] Yang, X., H. Zhang, J. Cai. Deconfounded Image Captioning: A Causal Retrospect. 45(11):12996–13010, 2023.
- [26] Wu, Z., Y. Xiong, S. X. Yu, et al. Unsupervised Feature Learning via Non-Parametric Instance Discrimination. In *Proceedings of the IEEE Conference on Computer Vision and Pattern Recognition*, pages 3733–3742. 2018.
- [27] Vaswani, A., N. Shazeer, N. Parmar, et al. Attention is All you Need. In *Advances in Neural Information Processing Systems*, vol. 30. Curran Associates, Inc., 2017.
- [28] Van Horn, G., O. Mac Aodha, Y. Song, et al. The INaturalist Species Classification and Detection Dataset. In *Proceedings of the IEEE Conference on Computer Vision and Pattern Recognition*, pages 8769–8778. 2018.
- [29] Kang, B., S. Xie, M. Rohrbach, et al. Decoupling Representation and Classifier for Long-Tailed Recognition. In *Eighth International Conference on Learning Representations (ICLR)*. 2019.
- [30] Wang, X., L. Lian, Z. Miao, et al. Long-tailed Recognition by Routing Diverse Distribution-Aware Experts. In *International Conference on Learning Representations*. 2020.
- [31] Cui, J., Z. Zhong, S. Liu, et al. Parametric Contrastive Learning. In *Proceedings of the IEEE/CVF International Conference on Computer Vision*, pages 715–724. 2021.
- [32] He, K., X. Chen, S. Xie, et al. Masked Autoencoders Are Scalable Vision Learners. In *Proceedings of the IEEE/CVF Conference on Computer Vision and Pattern Recognition*, pages 16000–16009. 2022.
- [33] Xu, Z., R. Liu, S. Yang, et al. Learning Imbalanced Data With Vision Transformers. In *Proceedings of the IEEE/CVF Conference on Computer Vision and Pattern Recognition*, pages 15793–15803. 2023.
- [34] Dosovitskiy, A., L. Beyer, A. Kolesnikov, et al. An Image is Worth 16x16 Words: Transformers for Image Recognition at Scale, 2021.
- [35] Touvron, H., M. Cord, H. Jégou. DeiT III: Revenge of the ViT. In S. Avidan, G. Brostow, M. Cissé, G. M. Farinella, T. Hassner, eds., *Computer Vision – ECCV 2022*, pages 516–533. Springer Nature Switzerland, 2022.
- [36] Yang, X., Y. Chen, X. Yue, et al. T-distributed Spherical Feature Representation for Imbalanced Classification. *Proceedings of the AAAI Conference on Artificial Intelligence*, 37(9):10825–10833, 2023.
- [37] Recht, B., R. Roelofs, L. Schmidt, et al. Do ImageNet Classifiers Generalize to ImageNet? In *Proceedings of the 36th International Conference on Machine Learning*, pages 5389–5400. PMLR, 2019.
- [38] Wang, H., S. Ge, Z. Lipton, et al. Learning Robust Global Representations by Penalizing Local Predictive Power. In *Advances in Neural Information Processing Systems*, vol. 32. Curran Associates, Inc., 2019.
- [39] Hendrycks, D., S. Basart, N. Mu, et al. The Many Faces of Robustness: A Critical Analysis of Out-of-Distribution Generalization. In *Proceedings of the IEEE/CVF International Conference on Computer Vision*, pages 8340–8349. 2021.
- [40] Ridnik, T., E. Ben-Baruch, A. Noy, et al. ImageNet-21K Pretraining for the Masses, 2021.
- [41] Wang, H., Z. Li, L. Feng, et al. Vim: Out-of-distribution with virtual-logit matching. In *Proceedings of the IEEE/CVF conference on computer vision and pattern recognition*, pages 4921–4930. 2022.
- [42] Cimpoi, M., S. Maji, I. Kokkinos, et al. Describing textures in the wild. In *Proceedings of the IEEE conference on computer vision and pattern recognition*, pages 3606–3613. 2014.

- [43] Van Horn, G., O. Mac Aodha, Y. Song, et al. The inaturalist species classification and detection dataset. In *Proceedings of the IEEE conference on computer vision and pattern recognition*, pages 8769–8778. 2018.
- [44] Huang, R., Y. Li. MOS: Towards Scaling Out-of-Distribution Detection for Large Semantic Space. In *Proceedings of the IEEE/CVF Conference on Computer Vision and Pattern Recognition*, pages 8710–8719. 2021.
- [45] Hendrycks, D., K. Zhao, S. Basart, et al. Natural Adversarial Examples. pages 15262–15271. 2021.
- [46] Wang, H., Z. Li, L. Feng, et al. ViM: Out-of-Distribution With Virtual-Logit Matching. pages 4921–4930. 2022.
- [47] Hendrycks, D., K. Gimpel. A baseline for detecting misclassified and out-of-distribution examples in neural networks. *arXiv preprint arXiv:1610.02136*, 2016.
- [48] Liu, W., X. Wang, J. Owens, et al. Energy-based out-of-distribution detection. *Advances in neural information processing systems*, 33:21464–21475, 2020.
- [49] Hendrycks, D., S. Basart, M. Mazeika, et al. Scaling out-of-distribution detection for real-world settings. *arXiv preprint arXiv:1911.11132*, 2019.
- [50] Sun, Y., C. Guo, Y. Li. React: Out-of-distribution detection with rectified activations. *Advances in Neural Information Processing Systems*, 34:144–157, 2021.
- [51] Lee, K., K. Lee, H. Lee, et al. A simple unified framework for detecting out-of-distribution samples and adversarial attacks. *Advances in neural information processing systems*, 31, 2018.
- [52] Li, J., P. Chen, Z. He, et al. Rethinking out-of-distribution (ood) detection: Masked image modeling is all you need. In *Proceedings of the IEEE/CVF conference on computer vision and pattern recognition*, pages 11578–11589. 2023.
- [53] Li, J., P. Chen, S. Yu, et al. MOODv2: Masked Image Modeling for Out-of-Distribution Detection. 46(12):8994–9003, 2024.
- [54] Lu, J., A. Liu, Y. Song, et al. Data-driven decision support under concept drift in streamed big data. *Complex & intelligent systems*, 6(1):157–163, 2020.
- [55] Wang, K., L. Xiong, A. Liu, et al. A self-adaptive ensemble for user interest drift learning. 577:127308, 2024.
- [56] Jiao, B., Y. Guo, D. Gong, et al. Dynamic Ensemble Selection for Imbalanced Data Streams With Concept Drift. 35(1):1278–1291, 2024.
- [57] Cerqueira, V., H. M. Gomes, A. Bifet, et al. STUDD: A student–teacher method for unsupervised concept drift detection. 112(11):4351–4378, 2023.
- [58] Yu, E., J. Lu, B. Zhang, et al. Online boosting adaptive learning under concept drift for multistream classification. In *Proceedings of the AAAI Conference on Artificial Intelligence*, vol. 38, pages 16522–16530. 2024.
- [59] Yu, E., Y. Song, G. Zhang, et al. Learn-to-adapt: Concept drift adaptation for hybrid multiple streams. 496:121–130, 2022.
- [60] Yu, H., W. Liu, J. Lu, et al. Detecting group concept drift from multiple data streams. 134:109113, 2023.
- [61] Li, W., X. Yang, W. Liu, et al. DDG-DA: Data Distribution Generation for Predictable Concept Drift Adaptation. 36(4):4092–4100, 2022-06-28.
- [62] Zhang, C., L. Zhang, D. Zhou. Causal Walk: Debiasing Multi-Hop Fact Verification with Front-Door Adjustment, 2024.
- [63] Miao, Q., J. Yuan, K. Kuang. Domain Generalization via Contrastive Causal Learning, 2022.
- [64] Yang, X., H. Zhang, G. Qi, et al. Causal Attention for Vision-Language Tasks. In *Proceedings of the IEEE/CVF Conference on Computer Vision and Pattern Recognition*, pages 9847–9857. 2021.
- [65] Chen, X., K. He. Exploring Simple Siamese Representation Learning. In *Proceedings of the IEEE/CVF Conference on Computer Vision and Pattern Recognition*, pages 15750–15758. 2021.

- [66] Wang, X., R. Zhang, C. Shen, et al. Dense Contrastive Learning for Self-Supervised Visual Pre-Training. In *Proceedings of the IEEE/CVF Conference on Computer Vision and Pattern Recognition*, pages 3024–3033. 2021.
- [67] Yang, X., L. Xu, H. Li, et al. Masked Image Contrastive Learning for Efficient Visual Conceptual Pre-training. *arXiv preprint arXiv:2411.09858*, 2024.
- [68] Yang, X., L. Xu, H. Sun, et al. Enhancing visual grounding and generalization: A multi-task cycle training approach for vision-language models. *arXiv preprint arXiv:2311.12327*, 2024.
- [69] Muennighoff, N., A. Rush, B. Barak, et al. Scaling Data-Constrained Language Models. 36:50358–50376, 2023.

Appendix

A Related Works

A.1 Concept Drift

In the comprehensive survey conducted by Lu et al. [7, 54], existing approaches for concept drift handling are systematically classified into three primary categories: error rate-based methods [55, 56], data distribution-based methods [8, 57], and multiple hypothesis-based techniques [58, 59]. Our proposed methodology falls under the category of distribution-based concept drift adaptation approaches. These distribution-driven techniques distinguish themselves by not only enabling precise drift identification through explicit statistical distribution analysis but also providing a multidimensional characterization of drift patterns - including temporal occurrence detection, affected feature space localization, and quantitative severity assessment. This dual capability of detection coupled with comprehensive drift diagnostics establishes distribution-based methods as particularly valuable for developing adaptive systems that require interpretable drift understanding and targeted model adjustments.

Besides, Online Boosting Adaptive Learning (OBAL) method [58] is proposed to address the challenges of concept drift and negative transfer in multistream classification. OBAL employs a dual-phase approach: an initial model is built using the Adaptive Covariate Shift Adaptation (AdaCOSA) algorithm to handle covariate shifts and learn dynamic correlations among streams. In the online phase, a Gaussian Mixture Model-based weighting mechanism is integrated to manage asynchronous drift. Meanwhile, CDMLLM [8] reveals that vision-language models suffer significant bias from concept drift during pre-training and fine-tuning. To address this, the authors propose a unified concept drift framework integrating T-distribution-based adaptation for long-tailed calibration and explicit OOD detection, demonstrating enhanced robustness in open-world multi-modal alignment through systematic distribution modelling. Beyond on drift detection in single data stream, GDDM [60] focuses on addressing group concept drift across multiple data streams, where individual drifts may go undetected due to subtle changes in underlying distributions. The proposed method introduces a distribution-free test statistic to detect concept drift in these complex scenarios. By designing an online learning algorithm for streaming data, the approach accurately identifies concept drift caused by hypothesis testing. Beyond that, DDG-DA [61] proactively models predictable factors influencing environmental evolution. The approach involves training a predictor to estimate future data distribution, using this information to generate training samples, and then training models on the generated data. By leveraging predictable factors to forecast data distribution changes, DDG-DA aims to enhance model performance in handling concept drift in streaming data. Furthermore, STUDD[57] proposes a teacher-student paradigm to enable unsupervised drift detection through deviation analysis of their predictive consistency. This approach leverages model disagreement as a proxy signal, bypassing dependency on ground-truth labels during deployment while maintaining detection sensitivity.

A.2 Causal Inference

Recently, increasing researchers have incorporated causal inference into deep-learning models, especially in large models. Deconfounded Image Captioning (DIC) [25] is proposed to address dataset bias in vision-language models through a causal lens, that integrates backdoor and front-door adjustments for systematic bias mitigation. The framework provides principled causal analysis of spurious correlations in multimodal alignment, offering theoretical grounding for decomposing bias sources through structured interventions. Likewise, aiming for spurious correlations induced by visual and linguistic biases during training, CIIC [24] is proposed as a causal intervention framework combining an Interventional Object Detector (IOD) and Interventional Transformer Decoder (ITD) guided by structural causal models. By applying backdoor adjustment through IOD’s feature disentanglement and ITD’s dual de-confounding mechanism, their approach systematically mitigates confounding effects across encoding and decoding stages, demonstrating enhanced generalization through causal correlation modeling. Similarly, targeting multi-hop fact verification bias in the large language model, Causal Walk [62] is proposed, a front-door adjustment framework that disentangles complex spurious correlations in evidence chains. The method models reasoning paths as mediators in structural causal models, decomposing causal effects via random walk-based treatment-mediator estimation and

geometric mean-based mediator-outcome approximation. By integrating adversarial and symmetric datasets synthesized with large language models, the approach demonstrates superior debiasing performance.

Additionally, causal inference is widely used in representation learning. Comprehensive Interventional Distillation (CID) [18] integrates causal intervention with class-aware representation alignment. By reinterpreting teacher logits as contextual confounders and applying counterfactual pruning through structural causal models, CID systematically disentangles beneficial semantic patterns from dataset-specific biases. This approach demonstrates enhanced generalization through bias-invariant knowledge transfer. Besides, De-confound-TDE [17] establishes a causal framework for long-tailed classification, identifying SGD momentum as a paradoxical confounder that simultaneously harms tail-class predictions while benefiting representation learning. Through causal intervention during training and counterfactual reasoning at inference, the method disentangles momentum’s detrimental bias from its beneficial mediation effects. Meanwhile, CCM [63] is proposed to address domain generalization through causal invariance principles. The framework integrates front-door adjustment with contrastive learning to quantify stable causal effects across domains, explicitly modeling domain shifts via a three-stage process: domain-conditioned supervision for feature correlation, causal effect measurement through structured path manipulation, and contrastive clustering for class-consistent representations. Similarly, CIRL [19] advances domain generalization through causal factorization, proposing a structural causal model that decomposes inputs into invariant causal mechanisms and domain-specific non-causal factors. It enforces three critical properties: causal/non-causal separation, joint independence, and causal sufficiency for classification.

Besides, C2L [20] addresses model fragility to spurious patterns through contrastive counterfactual synthesis, proposing a collective decision framework that aggregates predictions across generated counterfactual sets. Unlike conventional augmentation limited by dataset-inherent biases, this approach probabilistically supervises causal invariance through distributional consensus, demonstrating enhanced robustness against attribution bias and domain shifts. Furthermore, ABCD [21] establishes a causal interpretation of Transformer self-attention mechanisms, modeling them as structural equation estimators that capture conditional independence relations through partial correlation analysis in deep attention layers. This framework enables zero-shot causal discovery over input sequences while accounting for latent confounders, effectively repurposing pre-trained models for causal graph inference. What’s more, Causal Attention (CATT) [64] implements front-door adjustment to address confounding bias in attention mechanisms via dual-path processing of In-Sample and Cross-Sample Attention. By forcibly integrating external sample contexts through CS-ATT while maintaining standard attention conventions, CATT dynamically mitigates spurious correlations without requiring confounder specification.

A.3 Contrastive Pre-training

The seminal work of SimCLR [1] establishes foundational principles for contrastive pretraining through instance discrimination objectives and systematic augmentation strategies. While achieving remarkable performance in static environments, its reliance on fixed augmentation policies and stationary negative sampling assumes temporal consistency of latent patterns – an assumption violated under concept drift scenarios. Nevertheless, SimCLR’s demonstration of invariant representation learning through normalized temperature-scaled loss provides crucial architectural groundwork for developing drift-aware contrastive frameworks, particularly in modeling evolving feature relationships through dynamic positive/negative pair formulation.

Besides, the MoCo framework [3] and its subsequent evolution MoCo v3 [4] establish critical momentum-based mechanisms for contrastive learning through dynamic memory banks and stabilized key encoder updates. It is primarily designed to maintain consistency in negative sample maintenance and gradient stability. However, their fixed momentum schedules and stationary target assumptions limit adaptability to abrupt distribution shifts as we discussed aforementioned. Likewise, BYOL [9] employs two neural networks—an online network and a target network—that interact and learn from each other. Specifically, the online network is trained to predict the representation of an augmented image view produced by the target network, while the target network is updated using a slow-moving average of the online network’s parameters. Similarly, the SiamSim framework [65] advances contrastive representation learning through dynamic similarity calibration, employing a dual-path Siamese architecture with momentum-aligned feature projectors.

Meanwhile, DINO [5] and DINO v2 [6] advance self-distillation paradigms through momentum-based teacher-student mechanisms, leveraging global-local attention consistency in Vision Transformers to learn semantically structured representations. While achieving state-of-the-art in static self-supervised learning, their fixed teacher-student update schedules and monolithic prototype banks implicitly assume stationarity of feature distributions. DINO v2’s introduction of partitioned expertise through specialized sub-networks demonstrates partial adaptability to data variations, suggesting pathways for concept drift mitigation through dynamic expert routing. These works collectively establish critical baselines for stability-aware distillation architectures in non-stationary pre-training scenarios.

Furthermore, DenseCL [66] advances contrastive learning through localized feature alignment, introducing dense instance discrimination that operates at both image-level and pixel-level granularity. By enforcing spatial consistency through region-to-region contrastive pretext tasks, the method enhances model sensitivity to fine-grained visual patterns. While primarily designed for dense prediction tasks, its hierarchical contrast mechanism demonstrates the importance of multi-scale feature stabilization.

While contemporary contrastive pretraining methods achieve remarkable performance under static data distributions, their reliance on closed-world stationarity assumptions presents a fundamental limitation: they inherently lack mechanisms for concept drift adaptation when deployed in non-stationary environments with evolving data streams.

B Simple and Efficient Implementation with Scalability Advantages

Our RCP method is designed for simplicity and efficiency, integrating seamlessly with existing contrastive learning pipelines. As illustrated in Fig. 3, RCP requires only minimal modifications to standard architectures like MoCo v3 [4]. The primary adjustments involve incorporating our intervention module, which operates on the feature embeddings obtained from the student and momentum encoders. To support the larger effective batch sizes beneficial for capturing broader drift adaptation windows, we also leverage a masked contrastive strategy, inspired by recent work [67, 68].

Furthermore, RCP offers exceptional scalability advantages with respect to both data and model size. Firstly, it robustly accommodates diverse and expanding datasets during pre-training. By mitigating the adverse effects of concept drift, RCP ensures that model performance consistently benefits from increased data volume and variety, aligning with established scaling laws [69] without succumbing to drift-induced degradation. Secondly, RCP enhances the training stability of larger models in dynamic data environments. This improved stability facilitates the pre-training of models with significantly more parameters and deeper architectures, pushing the boundaries of what can be learned from evolving data streams.

C Experiments

In this section, we first introduce the details of utilized datasets for pre-training and various downstream tasks. Subsequently, implementation details are provided.

C.1 Datasets

ImageNet-LT [11] is a long-tailed subset derived from the ImageNet [10] dataset, designed to benchmark machine learning models under realistic class imbalance. It contains 115k training images across 1,000 categories, with class frequencies ranging from 1,280 (head classes) to merely 5 (tailed classes), simulating real-world data skewness. The validation set is balanced (20 images per class), while the test set aligns with the standard ImageNet validation data (50,000 images). It serves as a pivotal resource for studying long-tail recognition challenges, including few-shot learning, open-set generalization, and algorithmic fairness, while retaining compatibility with the original ImageNet hierarchy and evaluation protocols.

iNaturalist2018 [28] is a large-scale dataset designed to study fine-grained recognition under naturally occurring long-tailed class distributions. It comprises 675k training and validation images spanning 5,089 species hierarchically organized into 13 super-categories, with severe imbalance reflecting ecological rarity. The dataset integrates taxonomic metadata, geospatial coordinates, and temporal

Table 7: The pre-training hyperparameters.

	ViT-S/16	ViT-B/16	ViT-L/16
Training Epochs	800	800	800
Warmup Epochs	40	40	40
Optimizer	AdamW	AdamW	AdamW
Base Learning Rate	1.5e-4	1.5e-4	1.5e-4
Learning Rate Decay	Cosine	Cosine	Cosine
Adam β	(0.9, 0.95)	(0.9, 0.95)	(0.9, 0.95)
Weight Decay	0.05	0.05	0.05
Eff. Batch Size	32,000	9,600	2,400

annotations, supporting research in hierarchical learning, transfer learning, and self-supervised pretraining.

In terms of OOD detection, the Texture (DTD) [42] is a comprehensive collection of 5,640 texture images, meticulously organized into 47 categories based on human-centric perceptual attributes. Designed to support texture analysis and recognition tasks, DTD is divided into training, validation, and test sets, each containing 40 images per category. Besides, the iNat-OOD dataset [44] is a specialized subset of the iNaturalist [28] dataset, designed for evaluating out-of-distribution (OOD) detection methods in large-scale image classification tasks. The dataset is particularly valuable for testing the robustness of models in identifying novel or unseen categories, especially in ecological and biodiversity contexts. Meanwhile, ImageNet-O [45] is a specialized dataset designed to evaluate the robustness of visual models in detecting out-of-distribution (OOD) samples. It consists of 2,000 images from classes not included in the standard ImageNet-1k [10] dataset, making it a valuable benchmark for testing OOD detection methods. Additionally, OpenImage-O [46] is a large-scale, manually annotated dataset designed for out-of-distribution (OOD) detection tasks. It is derived from the OpenImage-V3 test set, which contains a diverse and natural distribution of images collected from Flickr without predefined class names or tags. This dataset aims to overcome the limitations of existing OOD benchmarks by providing a more realistic and challenging testbed for evaluating the robustness of computer vision models.

Regarding domain shift, ImageNet-V2 [37] is a comprehensive test set designed to evaluate the robustness and generalization of image classification models. It comprises 10,000 images, with 10 images per class, closely following the original labeling protocol of ImageNet. This dataset is instrumental in assessing how well models trained on the original ImageNet dataset can generalize to new, unseen data, making it a valuable resource for advancing computer vision research. The ImageNet-Sketch [38] is a unique collection of 50,000 hand-drawn sketch images, with 50 images for each of the 1,000 ImageNet classes. Constructed using Google Image queries, this dataset is designed to evaluate models' ability to learn out-of-domain semantics at the ImageNet scale. ImageNet-R [39] is a collection of 30k images representing 200 ImageNet [10] classes. These images are artistic renditions, including art, cartoons, graffiti, embroidery, origami, paintings, and other forms of creative expressions. The dataset is designed to test the robustness and generalization capabilities of image classification models when faced with non-standard inputs.

Table 8: The linear probing hyperparameters.

Downstream Tasks Models	Fine-tuning			Linear Probing		
	ViT-S/16	ViT-B/16	ViT-L/16	ViT-S/16	ViT-B/16	ViT-L/16
Training Epochs	100	100	50	90	90	50
Warmup Epochs	5	5	5	10	10	10
Optimizer	AdamW	AdamW	AdamW	LARS	LARS	LARS
Base Learning Rate	5e-4	5e-4	1e-3	0.1	0.1	0.1
Learning Rate Decay	Cosine	Cosine	Cosine	Cosine	Cosine	Cosine
Weight Decay	0.05	0.05	0.05	0.0	0.0	0.0
Eff. Batch Size	1,024	1,024	1,024	8,192	8,192	1,024

C.2 Implementation Details

We employ ViT-Small, ViT-Base and ViT-Large as our visual backbones, respectively. Among them, ViT-Base consists of 12 transformer encoder layers and an FFN intermediate size of 3,072. The hidden dimensions of the ViT-Base are 768, with 12 attention heads. The number of parameters is about 86 million. The input image size is set to 224×224 . For ViT-Small, ViT-S/16 comprises 12 transformer encoder layers with an FFN intermediate size of 1,536. The input image resolution is maintained at 224×224 , utilizing a patch size of 16×16 . The hidden dimension of ViT-Small is 384, featuring 6 parallel attention heads. The total parameter count approximates 22 million. In terms of the ViT-Large, ViT-L/16 consists of 24 transformer encoder layers and an FFN intermediate size of 4,096. The input image size is set to 224×224 , with a patch size of 16×16 . The hidden dimensions of the ViT-Large are 1,024, with 16 attention heads. And, the number of parameters is about 307 million.

In terms of the pre-training progress, the hyperparameters are presented in Table 7. We utilize the AdamW optimizer, which is configured with a cosine annealing schedule as the learning policy. The initial learning rate is set to 2×10^{-5} , and the AdamW optimizer is employed with hyperparameters $\beta = (0.9, 0.98)$. Additionally, we set the weight decay to 0.05 and the dropout rate to 0.1. During the first 40 warm-up epochs, the learning rate increases to 1.5×10^{-4} , and subsequently decays to 10^{-7} . Unless otherwise specified, the pre-training of our resilient contrastive model consists of 800, executed on 2×2 NVIDIA A100 GPUs.

While in the fine-tuning and linear probing on downstream task of classification, the hyperparameters are exhibited in Table 8. In the fine-tuning, the initial learning rate is 5×10^{-4} in ViT-S/16 and ViT-B/16, while 10^{-3} in ViT-L/16. Likewise, ViT-S/16 and ViT-B/16 need more training iterations with 100 epochs while 50 epochs within ViT-L/16, which are executed on 2×2 NVIDIA A100 GPUs.